Int. J. Solids Structures Vol. 25, No. 12, pp. 1427–1443, 1989
Printed in Great Britain.

0020-7683/89 $3.00 + .00
Pergamon Press plc

FLEXURAL BEHAVIOR OF STRAIN-SOFTENING SOLIDS

TZE-JER CHUANG and YIU-WING MAI†
Ceramics Division, National Institute of Standards and Technology,
Gaithersburg, MD 20899, U.S.A.

(*Received* 30 *October* 1988)

Abstract—The flexural behavior of a beam is investigated in an attempt to establish a correlation between the tensile and bending properties of strain-softening solids. Given the complete uniaxial stress–strain relations, including the post-peak tension-softening portion, it is possible to predict the flexural behavior in moment–curvature and load–deflection relations. The results indicate that strain-softening gives rise to enhanced bending strength in agreement with experimental data. Conversely, given the bending responses together with the softening characteristics the complete tensile behavior can be determined. Since bending experiments are easier to perform than uniaxial tensile tests, this well-defined correlation provides a feasible means to obtain the entire tensile behavior of strain-softening solids such as concrete, rocks and ceramics.

1. INTRODUCTION

The present paper is concerned with the flexural behavior of a class of strain-softening solids. It is now well established that many structural materials such as concrete, rocks and ceramics often display what is called "strain softening" behavior. See for example Read and Hegemier (1984), Bazant (1984), Gopalaratnam and Shah (1985), Shah and Sankar (1987), Reinhardt (1984), Dougill (1976), Krech (1974), Petersson (1981), Carpinteri (1985) and Roelfstra and Wittmann (1986). Basically, this means that in a direct tensile (or compressive) test there is a linear stress–strain relationship (Hooke's law) until the ultimate strength (σ_m) is reached. In reality, of course, there is a slight non-linearity prior to reaching σ_m, due to the development of microcracks randomly distributed within the body of the uniformly stressed solid. Further straining beyond this point results in stress relaxation which is the strain-softening characteristics of the material. From a physical point of view, this softening behavior is caused by the coalescence of densed microcracks within a narrow band (or softening zone width) of material. Outside this localized zone the rest of the material is effectively undergoing elastic unloading. It is possible to ascribe the decreasing stress bearing capacity in the softened material as due to the pulling out of aggregates from cement matrices in the case of concrete (Gopalaratnam and Shah, 1985); and of grain bridging and pull-out in the case of rocks and oxide ceramics (Mai and Lawn, 1986). One way to describe the strain concentration of the softening behavior is the adoption of a stress (σ)–crack opening displacement (δ) relationship using a fictitious single crack model (Reinhardt, 1984; Hillerborg *et al.*, 1976). Alternatively, an average strain (ε) on the continuum scale may be defined as representative of the opening displacement of the microcracks within an effective softening zone width (w_t). In this way, an effective stress–strain constitutive relationship can be adopted in the spirit of the "nonlocal continuum" concept (Bazant and Oh, 1983; Bazant and Chang, 1984). Of course, the crack opening displacement in the discrete crack model and the post-peak strain in the continuum model are then related by $\delta = w_t\varepsilon$. The present paper chooses the latter model to describe the strain-softening behavior.

In studying the fracture of strain-softening solids, knowledge of the tensile σ–ε (or δ) relationship is important, since this yields information on the fracture energy (G_f) consumed in the localized softened zone and also enables the crack growth resistance (R) curve to be numerically computed (Mai and Lawn, 1986; Foote *et al.*, 1986; Shah, 1986). In the past,

† On leave from the Department of Mechanical Engineering, University of Sydney, Sydney, N.S.W. 2006, Australia.

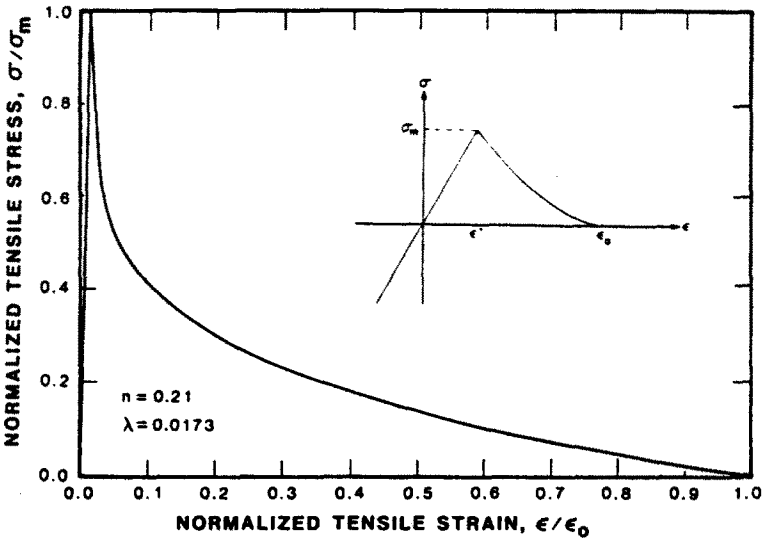

Fig. 1. Normalized plot of the assumed constitutive law [eqn (1)] with $n = 0.21$ and $\lambda = 0.0173$. The insert is a schematic showing the definitions of the relevant parameters (σ_m = tensile strength, ε^* = elastic strain at σ_m, ε_0 = fracture strain and $\lambda = \varepsilon^*/\varepsilon_0$).

considerable effort has been invested to design proper tensile experimentation in order to obtain the complete stress–strain curve including the post-peak regime. Particular attention has been given to specimen grip design, closed-loop strain control and testing machine stiffness (Gopalaratnam and Shah, 1985). In view of these complications, it is pertinent to ascertain whether such information can be extracted from bending test data, because bending experiments are more stable and easier to perform. In this paper we present a new analysis which establishes the relationship between tensile and bending properties of a class of strain-softening solids. It is shown that the bending load–displacement curves can be analytically predicted if the tensile strain–softening and fracture properties including the softening zone width are known (Section 2). Conversely, given the bending curve and the size of the accompanied fracture process zone development, the entire tensile properties can be determined (Section 3). Problems related to load instabilities and bending to tensile strength ratios as caused by the strain-softening zone width are also discussed.

2. ANALYSIS OF STRAIN-SOFTENING BEHAVIOR IN BENDING

The bending properties (i.e. moment–curvature, load–displacement and stress/strain distributions, etc.) of a uniform rectangular beam exhibiting the localized strain-softening phenomenon are analyzed in this section within the framework of a simple beam theory. The fundamental assumptions are given in Section 2.1.

2.1. *Basic assumptions*

In order to carry out the bending analysis, the constitutive laws for tension and compression of a beam element must be specified. A review on the strain-softening response of many engineering materials reveals that the stress–strain law follows a power-law function in the softening regime. The insert of Fig. 1 gives a schematic diagram of such a plot on which the current analysis is based. When $\varepsilon \leqslant \varepsilon^*$, where ε^* is the strain at which the softening behavior begins to develop, the elastic behavior dominates where the stresses vary linearly from zero to σ_m, the maximum tensile stress that the material can sustain. When $\varepsilon^* < \varepsilon < \varepsilon_0$, ε_0 being the separation strain (i.e. the strain at which fracture occurs), the material is in the strain-softening region where the tensile stress (σ) can be expressed empirically in the following power-law equation as a function of ε:

$$\sigma = \sigma_m\left[1-\left(\frac{\varepsilon-\varepsilon^*}{\varepsilon_0-\varepsilon^*}\right)^n\right], \quad 0<n<1, \tag{1}$$

where σ_m, ε^*, ε_0 and n are material constants. Finally, when the strain exceeds ε_0, complete separation of the softened material must have taken place.

The compression behavior, on the other hand, will be assumed linearly elastic regardless of the magnitude of stress, with an identical elastic modulus as in tension (i.e. $E = \sigma_m/\varepsilon^*$). This assumption is justifiable in view of the compression strength for many strain-softening solids is at least an order of magnitude higher than the corresponding tensile strength. For example, σ_m for a typical plain concrete is about 4 MPa in tension (Gopalarathnam and Shah, 1985), but about 40 MPa in simple compression (Shah and Sankar, 1987). Accordingly, the compression side of a bent beam is most likely in the elastic regime before fracture in the tensile zone intervened.

In order to formulate the load-point deflection in a general fashion, a segment of width $2w$ of the softening material is expected to occur in the mid-span of the beam whenever the strain of the outer-fiber in the tension side reaches ε^*. For a given material, beam geometry and loading configuration, this segment is expected to remain fixed (Bazant and Zubelewicz, 1988). In the present analysis, the width $2w$ is solved from the load-point deflection curve obtained in a bending experiment. As will be shown later, this localized softening zone width $2w$ will have a significant effect on the stability of the beam.

Also invoked in the present investigation is the well-known Bernoulli–Navier hypothesis wherein planar sections are assumed to remain plane under bending so that no warping takes place and compatibility requirement is automatically satisfied. The justification for strain linearization was first given by MacCollough (1933) in the case of creep deformation, where he argued that if non-linear bending strains were allowed to take place (i.e. warping) then either each individual element would respond differently for the same bending moment or they could not fit coherently together without creating discontinuity (i.e. violation of compatibility). Recently direct evidence of linear strain distribution in a ceramic beam was provided by Chuang *et al.* (1987). By putting two rows of identation marks in the midspan of a four-point bend bar, they were able to show that these two rows remained straight after a long period of creep deformation. Similar evidence was provided in the case of composite beams of reinforced concrete and steel-concrete (Barnard and Johnson, 1965), where the measured strain distributions are always linear but the corresponding stresses are non-linear and discontinuous. A direct observation on the strain field developed in a strain-softening solid poses an experimental challenge as the localized zone is so small as to render the measurements meaningless. However, indirect numerical calculations using the method of iterations do confirm this assumption of linear macrostrain distribution for strain-softening solids (Foote *et al.*, 1986; Wecharatana and Shah, 1983). In view of the similarities between strain-softening, creeping and fiber composite materials, in terms of non-linearity in stress and physical process involving microcracking and cavitation, coupled with confirmation of numerical calculations, we are led to believe that we have provided confidence in invoking Bernoulli's assumption, at least on the continuum scale, for the case of strain-softening behavior.

More recently, Bazant and Zubelewicz (1988) provided an exact nonlocal solution for a strain-softening beam under these two provisions. They derived the boundary conditions at the interface between the softening and the elastic regions and showed that these two assumptions are good representations of the real material behavior when compared to solutions obtained in local analysis. As the authors have correctly pointed out, some researchers at present do not believe that continuum models with strain-softening can adequately describe the physical reality. On the other hand, such an objection is clearly unfounded if a characteristic size w can be defined for the material, representing the crack band width.

The external loading mode considered in this paper is pertaining only to $\dot{\delta} > 0$, i.e. monotonically increasing displacement rate such as a constant cross-head speed as opposed to being load-controlled. This loading mode allows full details of the softening behavior to

be studied. Other loadings such as cyclic mode will not be considered here so as to avoid the complication of residual stresses.

2.2. *Bending analysis*

Because of the complexity of the constitutive laws (see Fig. 1), the bending properties of a beam specimen can be divided into three distinct regions each of which is analyzed separately in the following sub-sections. The analysis pertains to four-point bend configurations but other geometries of bending can also be equally applied as well.

2.2.1. *Elastic regime* (I). So long as the outer fiber strains in the inner span of the beam are less than ε^*, the beam is fully elastic and the associated deformation is completely reversible. The bending responses can be predicted within the framework of the conventional beam theory. At the end of the elastic regime (I) when the outer-fiber tensile strain reaches ε^*, the applied load and the load-point deflection can be expressed in terms of the beam geometry, σ_m and ε^*, as follows:

$$P_I^* = \tfrac{1}{3}\sigma_m BH^2/(L-l) \tag{2}$$

and

$$\delta_I^* = 2P_I^*(L-l)^2(L+2l)/(EBIl) = \tfrac{2}{3}\varepsilon^*(L-l)(L+2l)/H \tag{3}$$

where E is Young's modulus, $2L$ and $2l$ are the major and minor spans, respectively, and $B \times H$ is the cross-sectional area of the beam. In addition, the uniform curvature K inside the inner span is

$$K = 2\varepsilon^*/H \tag{4}$$

and from eqn (2) the corresponding applied moment is

$$M = \tfrac{1}{6}\sigma_m BH^2 \tag{5}$$

since $M = \frac{1}{2}P(L-l)$.

2.2.2. *Strain-softening zone growth regime* (II). When the load-point displacement, δ, exceeds δ_I^* defined in eqn (3), the beam undergoes a transition from the elastic regime (I) to the strain-softening zone growth regime (II), which can be defined as the loading period in which the outer-fiber strain of the softened material located in the inner span has the range $\varepsilon^* \leqslant \varepsilon \leqslant \varepsilon_0$. Note that the definition here is laid down in terms of *strain*, regardless of the level of the applied load, which may or may not exceed P_I^* depending on the specific constitutive law. To predict the flexural load versus deflection curve for a given $2w$ and σ–ε law (see Fig. 1) we need to know the moment versus curvature relationship for the softened beam element of width $2w$. In addition, we can also study the stability of a beam under constant displacement rate conditions. It will be shown that a critical zone width $2w_{cr}$ exists below which a sudden precipitious load drop is expected in the load–displacement curve (see Section 2.3.).

We begin the analysis of the softened zone by investigating first the normal stress distribution across the beam depth for an arbitrary curvature K in the regime. Figure 2

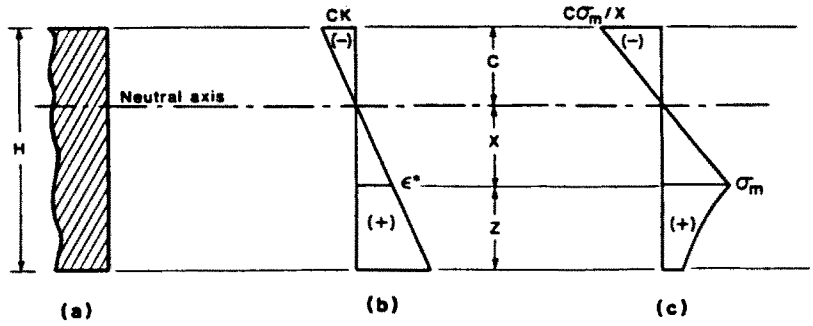

Fig. 2. Schematic of strain and stress distributions across the beam depth in regime (II).

shows the stress and strain distributions across the beam depth. In view of the linearity in strain (Fig. 2b) as assumed and discussed in Section 2.1, it is easy to show that the elastic tensile zone size X at a given K is

$$X = \varepsilon^*/K \tag{6}$$

from which the range of normalized X in regime (II) can be determined. Detailed derivations are given in Appendix A. The results are quoted here:

$$\frac{\lambda}{1+\sqrt{G}} < x < \tfrac{1}{2} \tag{7a}$$

or

$$2\lambda\varepsilon_0 < KH < \varepsilon_0(1+\sqrt{G}) \tag{7b}$$

based on the requirement that $\varepsilon_0 > \varepsilon > \varepsilon^*$ at the outer fiber in tension. Here, $x = X/H$ is the normalized elastic zone size and G is a material parameter defined by

$$G = \lambda(\lambda+2n-\lambda n)/(n+1) \tag{8}$$

where n is the exponent of the constitutive eqn (1) and λ $(= \varepsilon^*/\varepsilon_0)$ is the maximum elastic strain normalized against the separation strain ε_0 (see the insert of Fig. 1). The location of the neutral axis is at a distance $(X+Z)$ from the tensile face (see Fig. 2) where the softening zone depth Z is to be determined. For a fixed K, X is fixed by eqn (6) and Z can be computed from the following nonlinear algebraic equation:

$$z^{n+1} + B'z^2 - 2B'z + D' = 0 \tag{9a}$$

where

$$B' = x^{n-1}(1+n)(1-\lambda)^n/2\lambda^n \tag{9b}$$

and

$$D' = (1-2x)B'. \tag{9c}$$

Here $z = Z/H$ and eqn (9a) is derived from the condition of horizontal force balance so that the area of compressive stress (i.e. total compression force) must be equal to its counterpart in tension (see Fig. 2c). Closed-form solutions for Z in terms of X or K are available only when n is an integer and less than 4. In general, a numerical solution scheme has to be implemented, and there might be more than one solution. However, numerical search for the range of X which has physical meaning [eqn (7a)] indicated that only one solution for Z exists. Further, for small λ we found an approximate analytical solution:

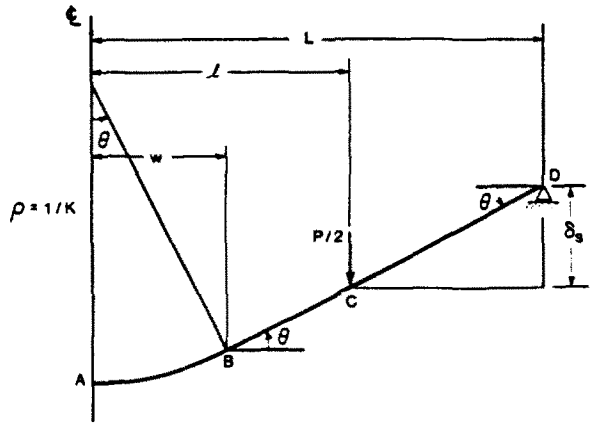

Fig. 3. Sketch of the right half of a deformed bend beam consisting of a softened part $\overline{AB}$ and a rigid portion $\overline{BCD}$ (vertical deflections are exaggerated for clarity).

$$z = 1-\sqrt{2x} \tag{10}$$

to underestimate the softening zone depth by about 9% at the end of the regime (II) (i.e. when the crack begins to form at the tensile face of the beam).

Once Z is solved, the position of the neutral axis is fixed for a given X or K. The bending constitutive law relating M to K can then be worked out by using moment balance equation $M = \int \sigma y \, dy$, where y is the distance away from the neutral axis. Thus, we obtain the following transcendental equations for the softened material of width $2w$:

$$\mathcal{M} = 2c^3/x + 2x^2 + 6xz + 3z^2 - 6\left\{\frac{\lambda}{1-\lambda}\right\}^n \frac{z^{(n+1)}}{x^n}\left\{\frac{x}{n+1} + \frac{z}{n+2}\right\} \tag{11a}$$

$$\kappa = \lambda/x \tag{11b}$$

where $c = 1-x-z$ is the normalized compression zone depth; $\mathcal{M} = M/(\frac{1}{6}\sigma_m BH^2)$ and $\kappa = KH/\varepsilon_0$ are the non-dimensional moment and curvature, respectively. The range of κ for regime (II) is $2\lambda \leqslant \kappa \leqslant (1+\sqrt{G})$, since $0.5 \leqslant x \leqslant \lambda/(1+\sqrt{G})$.

Having obtained the general expressions for the softening zone depth [eqns (9)–(10)] and bending moment [eqn (11)], the terminal values of Z and M at the end of regime (II) where $x = \lambda/(1+\sqrt{G})$ are readily available. Thus, inside this softened zone width of $2w$, the neutral plane is located at $(1+\sqrt{G})^{-1}$ from the tensile face of the beam, viz.

$$z = \frac{1-\lambda}{1+\sqrt{G}} \tag{12}$$

at the end of regime (II) and

$$\mathcal{M}_{II}^{*} = F/(1+\sqrt{G})^2 \tag{13a}$$

where

$$F = 3G + 2G\sqrt{G}/\lambda - \lambda^2 + 3n(1-\lambda)^2/(n+2). \tag{13b}$$

We can now predict the flexural load–displacement curve for a composite beam consisting of a central softening zone of width $2w$ and an elastic region of length $(L-w)$ on either side subject to four-point loading. Clearly, the load-point deflection has contributions from both the softening and elastic materials. To determine the contribution by the softening material alone, consider the schematic sketches shown in Fig. 3 where the beam is

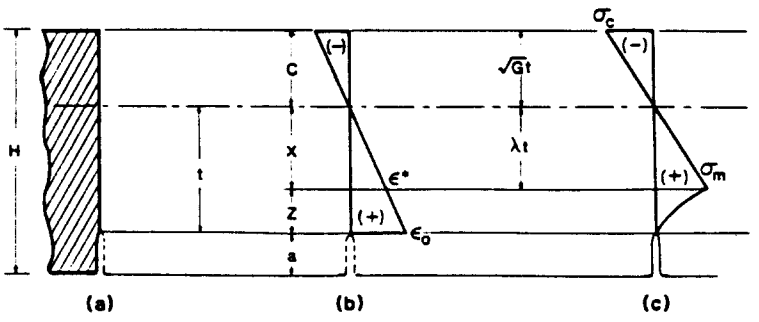

Fig. 4. Schematic of strain and stress distributions in the crack growth regime (III).

composed of a softening part ($\overline{AB}$) and a *rigid* material ($\overline{BCD}$). $\overline{AB}$ has the shape of a circular arc owing to the uniform curvature and $\overline{BCD}$ is a straight line because of its rigidity. From the geometry of the deformed beam, the load-point deflection is

$$\delta_s = (\hat{L}-\hat{l}) \tan [\arcsin (\hat{w}\kappa\varepsilon_0)] \tag{14}$$

where a chara on the top denotes normalized length against the beam height H (e.g. $\hat{L} = L/H$).

The elastic contribution to total δ from the portion of the part $\overline{BCD}$ can be evaluated using the method of strength of materials. By assuming $\overline{BCD}$ to be cantilever beam loaded by $P/2$ at C and at the free end D, the deflection can be worked out. The result is

$$\delta_e = \tfrac{2}{3}\lambda\varepsilon_0 \hat{w}/J \tag{15}$$

where

$$J = [(\hat{L}-\hat{w})^3 + 2(\hat{l}-\hat{w})^3 - 3(\hat{L}-\hat{w})(\hat{l}-\hat{w})^2]/(\hat{L}-\hat{l}). \tag{16}$$

Thus, the total deflection at the load-point is the summation of these two contributions, $\delta_s + \delta_e$, namely

$$\delta = (\hat{L}-\hat{l}) \tan [\arcsin (\hat{w}\kappa\varepsilon_0)] + \tfrac{2}{3}\lambda\varepsilon_0 \hat{w}/J. \tag{17}$$

This general expression for δ is applicable to a composite beam consisting of an elastic and a softening material. It is valid not only for regime (II) but also for the crack growth regime (III) to be discussed next.

2.2.3. *Crack growth regime*† (III). When the tensile edge of softened portion of the beam reaches ε_0, a crack will initiate there and the crack growth regime (III) ensues. The term "crack" here is defined as separation of "fiber" element rather than discontinuity in the continuum sense. Accordingly, any possible stress concentration near the "crack" tip is not considered here.

Figure 4 gives the schematic of stress and strain distributions in this regime. It might be noted that the stress distribution in the softened zone ahead of a crack as sketched in Fig. 4(c) is consistent with a blunt crack band model for softening behavior; its use being supported by the exact non-local solution as given by Bazant and Zubelewicz (1988). Also, note that the equality $c+x+z = 1$ no longer holds for this case. Instead, the normalized crack size a is defined as

† The definition of a "crack growth" regime is strictly incorrect because in addition to crack growth, the strain softening zone also exists albeit it is decreasing.

$$a = 1 - c - t \tag{18}$$

where t is the (normalized) tensile zone depth (Fig. 4c) resulting from the assumed strain distribution (Fig. 4b). Horizontal force balance derived in Appendix B, eqn (B5), then dictates that

$$c = \sqrt{G}\, t. \tag{19}$$

Setting $a = 0$ in eqn (18), we obtain the minimum curvature at which the initiation of crack growth occurs, i.e.

$$\kappa \geqslant 1 + \sqrt{G} \tag{20}$$

for regime (III).

We can also define the effective crack length, a^*, as $(a+z)$ in keeping with the definition used by many researchers. Thus we have

$$t = 1/\kappa \tag{21a}$$

$$a = 1 - (1 + \sqrt{G})/\kappa \tag{21b}$$

$$a^* = 1 - (\lambda + \sqrt{G})/\kappa \tag{21c}$$

for regime (III) where $\kappa \geqslant 1 + \sqrt{G}$. Further, fracture mechanics analysis permits use of the apparent stress intensity factor, K_I, in pure bending as a function of effective crack length a^*:

$$\hat{K}_I = \mathcal{M} Y(a^*) \tag{22a}$$

where $\hat{K}_I = K_I/(\sigma_m \sqrt{H})$ is the normalized K_I and Y is a dimensionless function of a^* given by Tada *et al.* (1973):

$$Y = \sqrt{2}\tan\left(\frac{\pi a^*}{2}\right)\left[0.923 + 0.199\left(1 - \sin\frac{\pi a^*}{2}\right)^4\right]\Big/\cos\left(\frac{\pi a^*}{2}\right). \tag{22b}$$

To obtain the normalized bending moment versus curvature relationship for the softening material in regime (III), the integral $\int \sigma y \, dy$ for the stress distribution in Fig. 4c has to be evaluated for $\mathcal{M}$. Mathematical manipulations given in Appendix B yield the following analytical expression relating $\mathcal{M}$ to κ:

$$\mathcal{M} = F/\kappa^2 \tag{23}$$

where F is a function of n and λ already defined in eqn (13b). This is a remarkably simple equation stipulating the moment-carrying capacity of the beam decayed asymptotically as the inverse square of deformed curvature. It should be pointed out that the transition point, $\kappa = (1 + \sqrt{G})$, which separates regimes (II) and (III), can be used to check the correctness of both analytical eqns (11a) and (23) and future numerical solutions in both regimes as they are independently derived. For example, substituting $\kappa = (1 + \sqrt{G})$ in eqn (23), we get an expression for $\mathcal{M}$ which agrees with that given by eqn (13a). This check assures the correctness of both eqns (11a) and (23) in regimes (II) and (III), respectively.

2.3. *Theoretical results*

We have presented in Section 2.2 the necessary equations for describing the flexural behaviors of a beam for all three characteristic regimes. We will now show the theoretical results using representative values of $n = 0.21$ and $\lambda = 0.0173$ for a particular polymer concrete studied by Krause (1980). Figure 1 gives a plot of the normalized stress versus

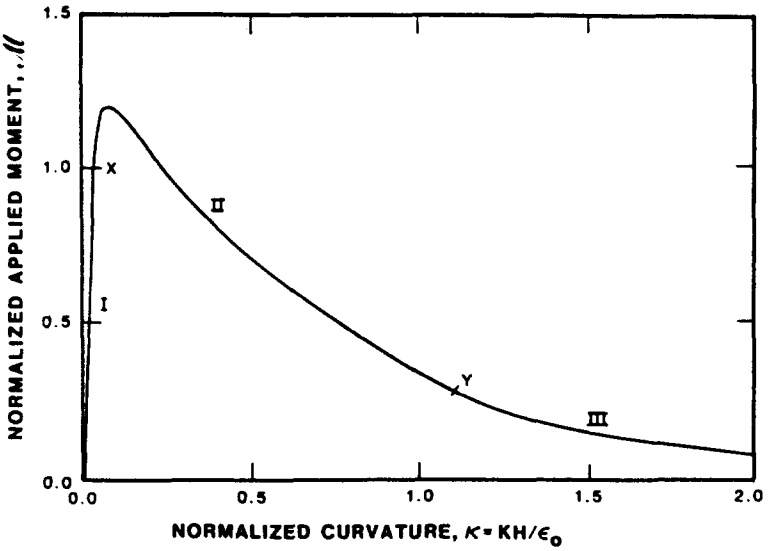

Fig. 5. Normalized plot of moment ($\mathscr{M}$) versus curvature (κ) for the strain-softened part of the beam for $n = 0.21$ and $\lambda = 0.0173$.

strain relation in simple tension based on eqn (1). The separation strain, ε_0, is about 58 times the maximum elastic strain, ε^*, demonstrating the enormous degree of ductility in the strain-softening zone for this material. With these values of n and λ we can proceed to evaluate the moment–curvature constitutive law for the softened material by using moment equations of (5), (11a) and (23) for the three different regimes. Equations (5) and (23) covering regimes (I) and (III) are analytical. But because there is no closed form solution for Z, eqn (11a) for $\mathscr{M}$ must be computed numerically for the regime (II). A FORTRAN subprogram has been developed to solve Z, the neutral axis location, for any given value of κ. The solutions are then used to compute $\mathscr{M}$ from eqn (11a). The final results are presented in Fig. 5 as a curve plotted in $\mathscr{M}$–κ space. The three stages are indicated in this figure. The two ends of regime (II), X and Y, are shown to agree with the terminating point and initiation point of regimes (I) and (III), respectively, in terms of both magnitude and slope, assuring the correctness of the numerical solution scheme developed for regime (II).

For engineering applications it is often required to determine the maximum load-bearing capacity of a given material. The peak load, P_m, or moment, $\mathscr{M}_m$, as shown in Fig. 5 for this polymer concrete is about 20% higher than the maximum elastic load. According to the definition of normalized $\mathscr{M}$ (i.e. $\mathscr{M} = M/\frac{1}{6}\sigma_m BH^2$) and eqns (2), (5) and the one immediately following eqn (5), the normalized peak load is identical to the peak moment, namely

$$\hat{P}_m \equiv P_m/P_l^* = \mathscr{M}_m. \tag{24}$$

To examine the bending strengths for a variety of materials with different sets of (n, λ) values, the curves of normalized peak moment, $\mathscr{M}_m$, as a function of the softening exponent, n, are plotted in Fig. 6 for three different values of λ. These curves show that increasing n leads to higher peak loads approaching the limiting value of 3.0 which represents the absolute maximum for bending strength. Reducing λ while keeping n constant yields similar results. This outcome can be physically explained in terms of the enhancement of the energy-absorbing capabilities for increasing n or reducing λ (see Fig. 1). Figure 6 also reveals that for strain-softening materials with $n > 0.1$, the ratio of bending strength to tensile strength is always greater than unity, namely $\mathscr{M}_m > 1.0$. These results are in good agreement with our experience in strain-softening materials like plain concrete. For "near" non-softening brittle materials with $n < 0.1$, the bending and tensile strengths are equal; no enhancement in bending strength is predicted.

One of our major objectives is to predict the flexural load–displacement curve from a given stress–strain relation such as the curves shown in Fig. 1. Treating the curvature as an

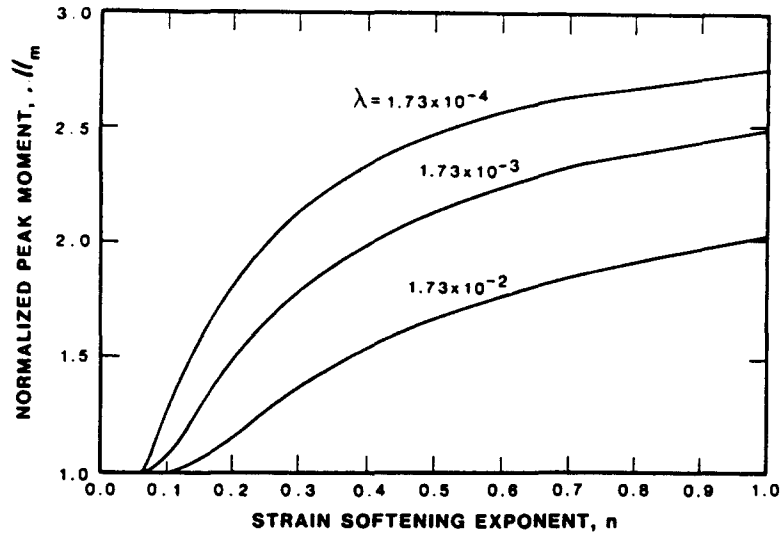

Fig. 6. Plot of strength enhancement in bending as a function of n for a trio of λ. Note that for exceedingly small n, no enhancement is predicted.

independent variable, the load and load-point displacement can be computed separately from eqns (11), (23) and (17) for a given material with fixed values of n and λ, specimen geometry and effective softened zone width $2w$. Figure 7 presents the normalized $\hat{P}$ vs δ curves for a trio of $\hat{w}$ in a special case wherein the material properties ($n = 0.21$, $\lambda = 0.0173$, $\varepsilon_0 = 0.0145$) and beam geometry ($\hat{L} = 4$, $\hat{l} = 1$) are fixed. The points X and Y on each curve divide the flexural behavior into the three regimes discussed earlier. It is interesting to note that the deviation from linearity in the P–δ curves at the commencement of regime (II) (i.e. point X) can be attributed to the development of the strain-softening zone. This prediction is consistent with the conventional understanding of microstructure in which microcracking introduces non-linearity if n exceeds 0.1. Further, this initial softening gives rise to strengthening in flexure as discussed earlier. Figure 7 also shows that the wider the softening zone, the larger the load-point displacement for a fixed load. In practice, the effective zone width $2\hat{w}$ can be estimated from the measured bending P–δ curve according to eqn (27) to be discussed later. In any event, three representative curves are plotted here: (1) for $\hat{w} = 0.15$, $d\delta > 0$ throughout the test; (2) $\hat{w}_{cr} = 0.09$, $d\delta = 0$ somewhere on the curve

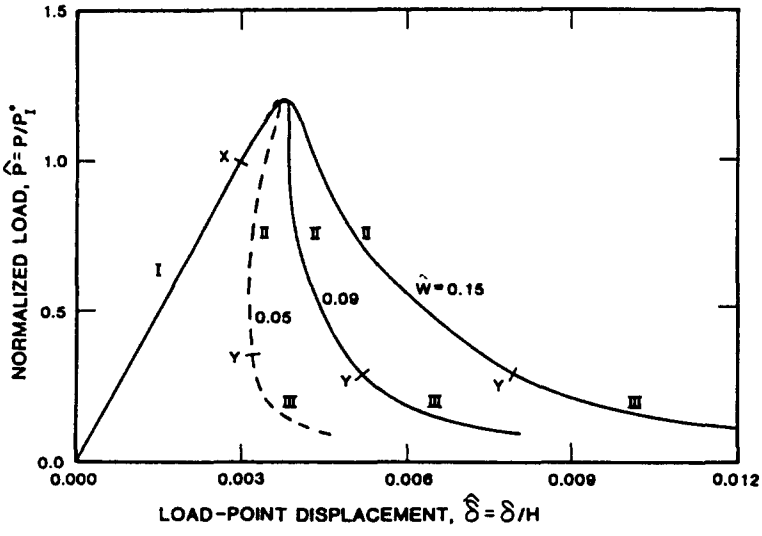

Fig. 7. Bending load-deflection diagrams for a trio of $\hat{w}$ showing how the softened zone size can affect the load stability conditions ($n = 0.21$, $\lambda = 0.0173$, $\varepsilon_0 = 0.0145$, $\hat{L} = 4$, $\hat{l} = 1$).

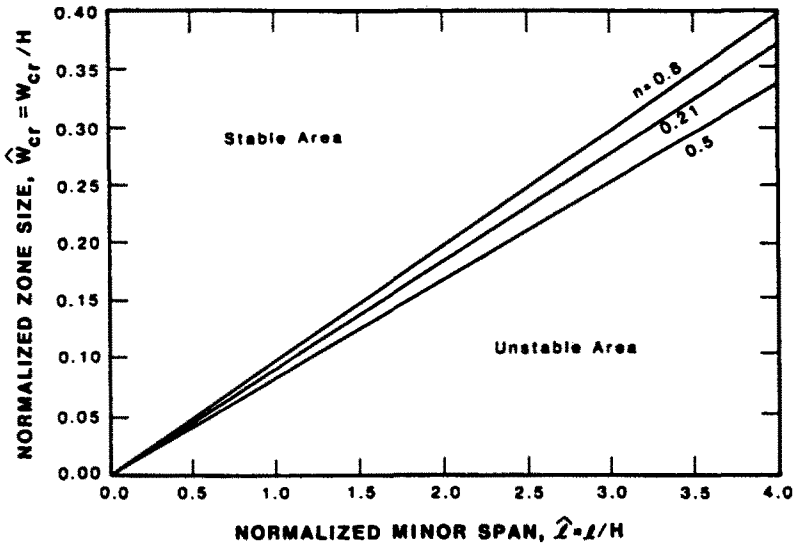

Fig. 8. Stability map for three different n values. For a given beam geometry, a larger softened zone provides a higher degree of stability; conversely, for a given w, a longer beam span produces less degree of stability ($\lambda = 0.0173$ and $\varepsilon_0 = 0.0145$).

such that there exists a vertical tangent on the P–δ curve; and (3) for $\hat{w} = 0.05$, $d\delta < 0$ for a portion of the curve indicating the test will be unstable for displacement-controlled loading conditions under which $d\delta$ has to be positive. In this last case, the part of the curve for which $d\delta < 0$ cannot be recorded and instability (i.e. a sudden drop in load) will result. This prediction seems to agree with P–δ curves observed on mortar beam specimens using a new loading system where the controlling parameter is the differential signal between a load and a displacement (Rokugo *et al.*, 1986; Carpinteri, 1985).

To further understand the stability conditions, a comprehensive map (Fig. 8) can be constructed where areas of stable and unstable regions in the $\hat{w}$–$\hat{l}$ space are separated by a critical border line depending on the material parameter n. Three interesting results are in order. Firstly, for a fixed $\hat{w}$ larger beams spans yield less degree of stability presumably because larger beams spans store more elastic energy. This is consistent with the experimental observations of P–δ bending curves on mortar (Carpinteri, 1985; Rokugo *et al.*, 1986). Secondly, for a fixed value of n, the boundary separating these two areas is a straight line. Finally, the boundary line corresponding to $n = 0.5$ has the least slope meaning a material with a softening exponent of one half will provide the most stable loading conditions since this case generates the largest stable area on the map.

The evolution of the crack and strain-softening zone growth as the load-displacement is increased can now be studied using eqns (21b) and (21c). Take polymer concrete (i.e. $n = 0.21$, $\lambda = 0.0173$) as an example, we plot in Fig. 9 the depth of the strain-softening zone (Z), the nominal and effective crack lengths, a and a^*, as a function of the curvature κ. It is seen that a^* is rising rapidly at the initial stage and then tapers off as the curvature increases to values higher than unity. Thence onwards a hinge mechanism is effectively activated under which deformation is allowed to continue without changing the load substantially. Real crack growth does not take place until the softened zone has grown well over 90% of the beam depth (in this particular example chosen). Once the crack is initiated at the tensile edge it grows rapidly while the softened zone is predicted to decrease.

The conventional fracture toughness, K_I, of a beam as a function of effective crack length,† a^*, can also be calculated using eqns (22). Figure 10 gives such a "R-curve" where K_I is seen to increase gradually from zero to a peak value at about 10 times $\sigma_m\sqrt{H}$, and then to decrease rapidly to zero‡ as the crack grows across the beam depth. The latter is a

† Here, we treat the softening zone as a non-linear fracture process zone ahead of the real crack tip. Linear elastic fracture mechanics formulae can still apply by calculating K_I at the tip of the softened zone.

‡ It can be shown mathematically from eqn (22b) that $\lim_{a \to 1} Y(a) = 0$ so that $K_I = 0$ when $a = H$.

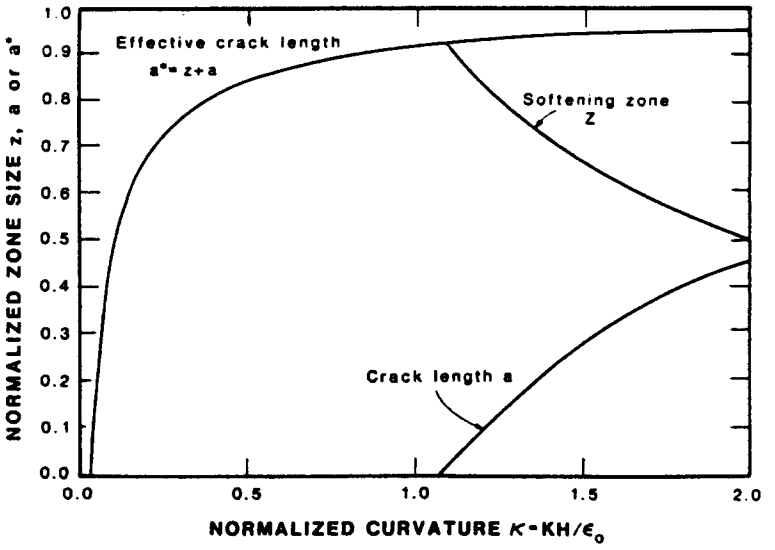

Fig. 9. Growth of Z, a and a^* as a function of κ for $n = 0.21$ and $\lambda = 0.0173$.

manifestation of the decreasing load required coupled with the constraint placed on the growth of the softening zone by the free boundary of the back face of the beam.

3. THE INVERSE PROBLEM

3.1. *Extracting tensile properties from bending curve*

Thus far, we are able to predict the bending load–deflection curve when the geometry and σ–ε laws of the beam, including the softening zone width, are given. We now raise a practical issue: can we solve the *inverse* problem? That is, given a flexural load–displacement curve, can we obtain the materials' strain-softening response in tension? This problem is of significant importance as mentioned in Section 1. For if it is possible, we need only do the simple bending experiments as opposed to the far more complicated tensile test in order to extract the tensile softening properties, which in turn may be used for structural analyses.

From the flexural P–δ curve measured in the laboratory, we can obtain the following quantities: (1) P_I^*, the point of deviation from the linear curve of regime (I); (2) P_{I_y}, the

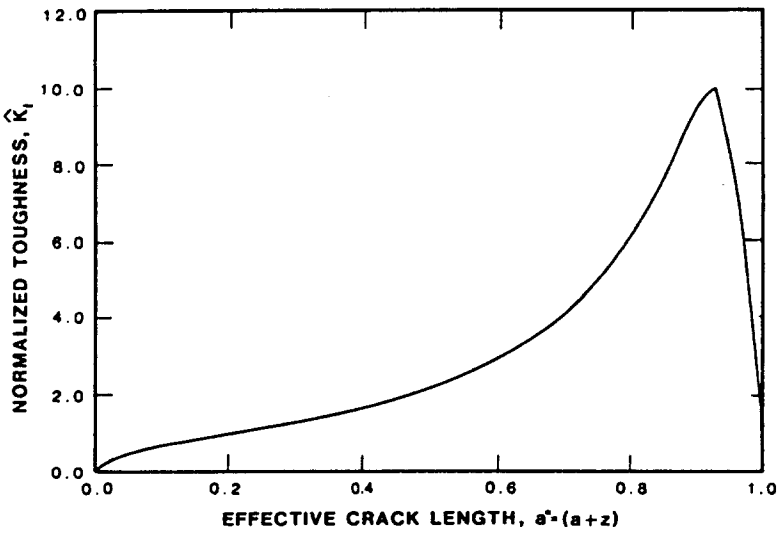

Fig. 10. Evolution of fracture resistance in regime (III) for $n = 0.21$ and $\lambda = 0.0173$, indicating R-curve behavior.

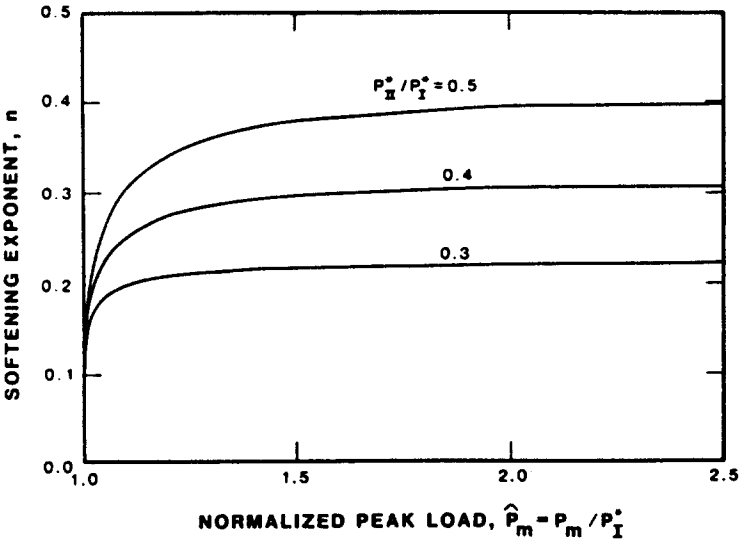

Fig. 11. Effect of n on the normalized peak load, $\hat{P}_m$, for three values of P_{II}^*/P_I^*.

peak load; (3) the entire tail curve in regime (III); (4) P_{II}^*, the point of departure from the tail curve in regime (III) as defined by eqn (25); and (5) the corresponding displacement δ_{II}^*. The information from (1), (2) and (4) provides the values of the normalized moments $\mathcal{M}_m$ and $\mathcal{M}_{II}^*$. The information from (3) gives a clue as to the applicability of the present theory because it predicts the P–δ curve to assume the following quadratic form:

$$\hat{P} \cong F\varepsilon_0^2\hat{w}^2(\hat{L}-\hat{l})^2/\delta^2 \tag{25}$$

based on eqns (17) and (23). Indeed, Yan (1988) of AT&T Bell Laboratories has plotted the post-peak P–δ curve of a fiber-reinforced glass preform on a log–log paper and found that a portion of the data at the tail end did decay linearly with a slope of -2.2 which is close to the theoretical value of -2 according to eqn (25). Furthermore, he was able to locate the point Y separating regimes II and III as defined in Fig. 5 at the point of deviation from the straight line.

Now from Fig. 6, we have the following *numerical* relation

$$\mathcal{M}_m = f(\lambda, n)$$

and from eqn (13a),

$$\mathcal{M}_{II}^* = F/(1+\sqrt{G})^2.$$

These two equations form a system of non-linear algebraic equations for the unknown parameters λ and n. The task is to solve them as a function of $\mathcal{M}_m$ and $\mathcal{M}_{II}^*$ which are prescribed by the test data. Because of the lack of an analytical expression for the first equation, the problem is solved numerically by the Newton–Raphson iterative method. In general, unique solutions are not guaranteed for non-linear problems. However, numerical searching in the range of physical interest, namely $P_{II}^*/P_I^* = 0.1 \sim 0.7$, reveals that unique solutions exist in this range. Figures 11 and 12 give the solution for n and λ for $P_{II}^*/P_I^* = 0.3$, 0.4 and 0.5, respectively. From Fig. 11, it is noted that n varies in a narrow range between 0.2 and 0.4. Furthermore, for a given value of P_{II}^*/P_I^*, the peak load P_m is very sensitive to changing n. Conversely, the solutions for λ vary widely from 0.5 down to 10^{-5} when the normalized peak loads increase from 1.0 to 2.2, Fig. 12. In the following Section 3.2, we demonstrate the use of these solutions in an example, where the flexural P–δ curves are measured, so as to obtain the simple tension behavior of the particular material. Once n and λ are determined, the complete tensile σ–ε curve including σ_m, ε^* and ε_0 can be obtained

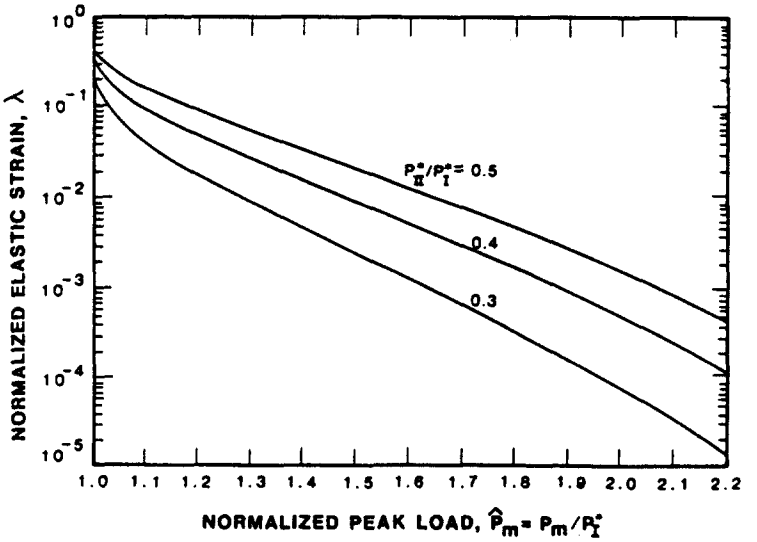

Fig. 12. Solutions of λ as a function of $\hat{P}_m$ for three values of P_{II}^*/P_I^*.

from the information gathered at P_I^*. To convert the tensile σ–ε relation to the σ–δ curve, the softening zone width w_t in tension is required. To estimate w_t, consider a tensile specimen of unit cross-sectional area containing a localized strain-softened zone width w_t, energy balance at fracture requires that $G_f = w_t \int \sigma \, d\varepsilon$. Integration of the σ–ε curve on the softening part, assuming the elastic portion is negligible, gives

$$w_t = G_f(n+1)/(1-\lambda)\sigma_m\varepsilon_0 n. \tag{26}$$

The crack opening displacement δ is simply related to the effective strain ε within the fracture process zone by $\delta = \varepsilon w_t$ and the complete tensile σ–δ curve is thus obtained.

It should be pointed out that although w in bending and w_t in tension may have the same order of magnitude, say a few millimeters, they are not necessarily equal because w_t is material dependent only [see eqn (26)] while w may also involve specimen geometry and loading configuration [see eqns (17) and (27) below]. Given δ_{II}^* from the measured P–δ curve in a bending experiment, the effective softened zone width $2w$ can be estimated at that point on the curve. Thus, for $\delta = \delta_{II}^*$, eqn (17) then gives

$$w = H\delta_{II}^*/(L-l)(1+\sqrt{G})\varepsilon_0 - \tfrac{2}{3}\lambda F(L^3+2l^3-Ll^2)/(1+\sqrt{G})^3(L-l)^2. \tag{27}$$

It is seen that if $\hat{w}$, ε_0 and $\kappa \ll 1$, the bending softening zone width is then linearly dependent on δ_{II}^*.

3.2. *Example on polymer concrete*

Here we use polymer concrete as an example to demonstrate the procedure of extracting the tensile softening behavior from the laboratory measured load–deflection curve in bending. Flexural load–displacement diagrams for a polymer concrete have been previously obtained (Krause, 1980; Krause and Fuller, 1984). To deduce the tensile σ–δ curve from P–δ curves measured by a four-point bend method, the first step is to obtain a pair of (n, λ) from Figs 11 and 12. The required information are P_m, P_{II}^* and P_I^* from the load–deflection diagram. For the polymer concrete studied by Krause and Fuller (1984), the values of P_m and the ratio P_{II}^*/P_I^* are estimated to be 1.2 and 0.3, respectively. Thus, from Fig. 11 we obtain $n = 0.2$ and from Fig. 12, $\lambda = 0.0173$. The next step is using the information on P_I^* and δ_I^* obtained and the known beam geometry to calculate σ_m and ε^* from eqns (2) and (3). This gives $\sigma_m = 19.4$ MPa and $\varepsilon^* = 250$ μ strain. The complete σ–ε curve in tension including the post-peak region is now determined. To obtain stress–displacement curve in tension, we need to know the softening zone width w_t. So the final step is to calculate w_t

from a given G_f according to eqn (26). Assuming $G_f = 50$ J m^{-2} for the polymer concrete (Krause and Fuller, 1984), the zone width w_t is then calculated to be about 1.05 mm. With w_t known, we are able to convert the σ–ε curve into the σ–δ curve, since δ and ε are related by $\delta = w_t\varepsilon$. Unfortunately, no data on the σ–δ curve are available for the polymer concrete so that verification of this prediction cannot be made at this time. However, the peak load $\sigma_m = 19.4$ MPa predicted is in very good agreement with the tensile strength data of 18 ± 2.4 MPa measured by Krause (1980) using the direct splitting technique.

4. SUMMARY

We have presented a detailed investigation into the flexural behavior of a composite beam containing a localized strain-softening zone. Three characteristic regimes are identified for increasing strain conditions: (I) elastic (II) strain-softening zone growth and (III) crack growth. It is shown that enhanced bending strength occurs at regime (II) provided the strain-softening exponent (n) exceeds ≈ 0.1 and that the softening zone width ($2w$) has a significant influence on the load stability in bending experiments. The fracture resistance is also shown to increase in regime (III) as a function of crack length consistent with the conventional R-curve concept.

We also presented the solutions for the inverse problem, namely, the determination of the stress–displacement relations in simple tension from simple bending data. The solution depends on two load ratio measurements: $\hat{P}_m$ and P_{II}^*/P_I^*. An example on polymer concrete is employed to illustrate the step-by-step procedure in the acquisition of the final σ–δ relationship in tension. We believe that the present work provides a simple but very useful technique to characterize a class of strain-softening solids which obey the constitutive law given in eqn (1). Obviously, much future experimental work is required to substantiate the theoretical analysis.

Acknowledgements—We are grateful to J. T. Fong of the Center for Computer and Applied Mathematics, NIST, for critically reviewing the manuscript. One of us (Y.-W. Mai) also wishes to thank the Australian Research Council for financial support.

REFERENCES

Barnard, P. R. and Johnson, R. P. (1965). Ultimate strength of composite beams. *Inst. Civil Eng.* **32**, 161–179.

Bazant, Z. P. (1984). Imbricate continuum and progress fracturing of concrete and geomaterials. *Mechanica* **19**, 86–93.

Bazant, Z. P. and Chang, T.-P. (1984). Instability of nonlocal continuum and strain averaging. *J. Eng. Mech.* **110**, 1441–1450.

Bazant, Z. P. and Oh, B. H. (1983). Crack band theory for fracture of concrete. *Mater. Struct.* **16**, 155–177.

Bazant, Z. P. and Zubelewicz, A. (1988). Strain-softening bar and beam: exact non-local solution. *Int. J. Solids Structures* **24**, 659–673.

Carpinteri, A. (1985). Interpretation of the Griffith instability as a bifurcation of the global equilibrium. In *Application of Fracture Mechanics to Cementitious Composites* (Edited by S. P. Shah), pp. 287–316. Martinus Nijhoff, Dordrecht.

Chuang, T.-J., Wiederhorn, S. M. and Chen, C. F. (1987). Transient behavior of structural ceramics under flexural creep. In *Creep and Fracture of Engineering Materials and Structures* (Edited by B. Wilshire and R. W. Evans), pp. 957–973. The Institute of Metals, London.

Dougill, J. W. (1976). On stable progressively fracturing solids. *J. Appl. Math. Phys.* (ZAMP) **27**, 423–437.

Foote, R. M. L., Mai, Y.-W. and Cotterell, B. (1986). Crack growth resistance curves in strain-softening materials. *J. Mech. Phys. Solids* **34**, 593–607.

Gopalaratnam, V. S. and Shah, S. P. (1985). Softening response of plain concrete in direct tension. *ACI Jl* **82**, 310–323.

Hillerborg, A., Modeer, M. and Peterson, P. E. (1976). Analysis of crack formation and crack growth in concrete by means of fracture mechanics and finite elements. *Cement Concrete Res.* **6**, 773–782.

Krause, R. F. (1980). Testing geothermal well cements: strength measurements following exposure to simulated geothermal fluids. NBS Internal Report No. 80-20994.

Krause, R. F. and Fuller, E. R. (1984). Fracture toughness of polymer concrete materials using chevron-notched configurations. In Chevron-notched specimens: testing and stress analysis, ASTM STP 855, 309–323, Philadelphia.

Krech, W. W. (1974). The energy balance theory and rock fracture energy measurements for uniaxial tension. In *Proc. 3rd Int. Soc. Rock Mech. Congress*, Vol. 2A, Denver.

MacCollough, G. H. (1933). An experimental and analytical investigation of creep in bending. *Trans. ASME (Appl. Mech.)* **1**, 55–60.

Mai, Y.-W. and Lawn, B. R. (1986). Crack stability and toughness characteristics in brittle materials. *A. Rev. Mater. Sci.* **16**, 415–439.
Petersson, P.-E. (1981). Crack growth and development of fracture zones in plain concrete and similar materials. Report No. TVBM-1006, Lund Inst. Technology, Lund, Sweden.
Read, H. E. and Hegemier, G. A. (1984). Strain softening of rock, soil and concrete—a review article. *Mech. of Mater.* **3**, 271–294.
Reinhardt, H. W. (1984). Fracture mechanics of an elastic softening material like concrete. *HERON* **29**, 3–42.
Reinhardt, H. W. (1985). Crack softening zone in plain concrete under static loading. *Cement Concrete Res.* **15**, 42–52.
Roelfstra, P. E. and Wittmann, F. H. (1986). Numerical method to link strain softening with failure of concrete. In *Fracture Toughness and Fracture Energy of Concrete* (Edited by F. H. Wittmann), pp. 165–175. Elsevier, Amsterdam.
Rokugo, K., Ohno, S. and Koyanagi, W. (1986). Automatical measuring system of load–displacement curves including post-failure region of concrete specimens. In *Fracture Toughness and Fracture Energy of Concrete* (Edited by F. H. Wittmann), pp. 403–411. Elsevier, Amsterdam.
Shah, S. P. (Ed.) (1986). *Applications of Fracture Mechanics to Cementitious Composites*. Martinus Nijhoff, Dordrecht.
Shah, S. P. and Sankar, R. (1987). Internal cracking and strain-softening response of concrete under uniaxial compression. *ACI Mater. Jl* **84**, 200–212.
Tada, H., Paris, P. C. and Irwin, G. R. (1973). *The Stress Analysis of Cracks Handbook*, pp. 2–14. Del Research Corporation, Hellertown, PA.
Wecharatana, M. and Shah, S. P. (1983). Predictions of nonlinear fracture process zone in concrete. *J. Engng Mech.* **109**, 1231–1245.
Yan, M. F. (1988). Private Communication.

APPENDIX A: RANGE OF X IN REGIME II

We wish to derive here the range (i.e. the upper and lower limits) of the elastic tensile zone size X (see Fig. 2). At the end of regime II the strain at the outer tensile fiber must be ε_0 so that a major crack is about to initiate there. Designating Y as the total tensile zone size, $Y = X + Z$, we have

$$K = \frac{\varepsilon^*}{X} = \frac{\varepsilon_0}{Y}.$$

Hence,

$$x = \lambda y \tag{A1}$$

since $\lambda = \varepsilon^*/\varepsilon_0$. Horizontal force balance then requires that

$$\tfrac{1}{2}c^2\sigma_m/x = \sigma_m x/2 + \frac{n}{n+1}\sigma_m(y-x)$$

or

$$(1-y)^2 = x^2 + \frac{2nx}{n+1}(y-x).$$

By noting that $x = \lambda y$ from eqn (A1), these results are simplified to

$$x = \lambda/(1+\sqrt{G}) \tag{A2}$$

where G has already been defined in eqn (8) of the text.

On the other hand, at the beginning of regime II or at the end of regime I, $z = 0$ and $x = c = \frac{1}{2}$ so that neutral axis is still at, but about to move from, the center of the cross-section.

Hence we have derived the limits of x in regime II to be as follows

$$\frac{\lambda}{1+\sqrt{G}} < x < \tfrac{1}{2}$$

as indicated in eqn (7a) of the text.

APPENDIX B: DERIVATION OF EQN (23)

Referring to Fig. 4(b), the tensile zone size, t, is given by

$$t = \varepsilon_0/K \tag{B1}$$

owing to strain linearization. Also, from Fig. 4(c), it is clear that a relationship between σ_c and σ_m can be established:

$$\sigma_c/c = \sigma_m/\lambda t. \tag{B2}$$

The total compression force per unit thickness of the beam acting on the section is

$$F_c/B = \tfrac{1}{2}\sigma_c c = \tfrac{1}{2}\sigma_m c^2/\lambda t \tag{B3}$$

after substituting σ_c from eqn (B2). On the other hand, the total tension force per unit thickness of the beam acting over the whole section is

$$F_t/B = \tfrac{1}{2}\sigma_m \lambda t + \frac{n}{n+1}\sigma_m(1-\lambda)t \tag{B4}$$

after integration of tensile stresses over both the linear and non-linear parts. Equating the above two equations, owing to the requirement of equilibrium we obtain

$$c = (\sqrt{G})\, t \tag{B5}$$

where G is defined by eqn (8).

In addition, the equilibrium conditions also demand that internal moment be counter-balanced by the applied moment. Thus, by taking the moment at the neutral axis for internal stresses and equating this to the applied moment M, we have

$$M/B = (F_c/B)\cdot \tfrac{2}{3}c + \tfrac{2}{3}(\tfrac{1}{2}\sigma_m \lambda^2 t^2) + \left(\frac{n\sigma_m(1-\lambda)t}{n+1}\right)\left[\lambda t + \frac{(n+1)(1-\lambda)t}{2(n+2)}\right].$$

Substitution of c from eqn (B5), t from eqn (B1) and F_c from eqn (B3) into the above equation gives

$$M/(\tfrac{1}{6}BH^2\sigma_m) = \left[\frac{2G\sqrt{G}}{\lambda} + 3G - \lambda^2 + \frac{3n(1-\lambda)^2}{n+2}\right] \Big/ (KH/\varepsilon_0)^2$$

or

$$\mathcal{M} = F/\kappa^2 \tag{B6}$$

where F is defined by eqn 13(b). Equation (B6) is then equal to eqn (23) in the text.